Comparative Validation of Light Environment Simulation with Actual Measurements

Juhyang Park, Kyungsun Lee * and Kirim Kim

School of Architecture, Hongik University, Seoul 04066, Republic of Korea; c2111113@g.hongik.ac.kr (J.P.); kkl881008@g.hongik.ac.kr (K.K.)
* Correspondence: ksunlee@hongik.ac.kr; Tel.: +82-10-3731-2170

Abstract: The quality of indoor lighting significantly influences human well-being, emphasizing the need to integrate lighting planning into the architectural design process. To optimize indoor lighting conditions, light environment simulations are commonly employed. While much of the relevant literature clearly shows that simulations are widely used to predict lighting environments, there is limited active research validating these simulations. Therefore, this study aimed to assess the alignment between actual measurements and simulations, specifically focusing on daylight-induced glare. To achieve this, a comparative analysis and verification of glare levels between simulations and actual measurements were conducted that accounted for glare location and direction. Disparities between the simulated and measured glare levels were revealed contingent on the glare location and direction. These variations primarily arose from the simulation's utilization of a fisheye field of view (FOV) for glare measurement. To improve the accuracy of glare analysis in simulations, it is advisable to follow the standards related to the human perception of glare, such as the human field of view (FOV), instead of solely depending on a fisheye FOV. The study's limitations include challenges in environmental replication, minor measurement errors, and tree branch shading interference. Despite the potential for simulations to not replicate temporary glare effects, consistent differences with actual measurements indicate that the fisheye FOV was a key contributing factor.

Keywords: indoor light environment; luminance; glare; actual measurement; simulation; workspace

1. Introduction

In modern society, light wields a profound influence on human physiology and psychology, making it a pivotal environmental factor for enhancing health and well-being [1–5]. As the majority of individuals now predominantly remain indoors, the need arises to meticulously craft lighting environments tailored to specific indoor spaces [6]. These spaces encompass residential, educational, and work-oriented spaces, each of which entails extended indoor stays, thus necessitating comprehensive lighting environment planning. Notably, individuals in workspaces are acutely sensitive to prolonged exposure to the lighting environment, which significantly affects work efficiency, worker health, and overall satisfaction [7].

The strategic development of an optimal lighting environment relies on precise measurement and evaluation techniques. Two primary methods are employed for light environment measurement: utilizing measuring equipment in actual spaces and conducting computer-based 3D modeling simulations [8]. While measurement devices offer precise assessments of luminance, color rendering, and illuminance, their application is confined to spaces that are already constructed. In contrast, simulations enable the modeling of various scenarios in virtual environments, proving invaluable during the initial design phases [9]. However, it should be recognized that simulations can exhibit deviations when compared to actual measurements [8].

The evaluation of the light environment yields crucial insights into its impact on psychological comfort and physical health, based on factors such as luminance, color

rendering, and illuminance obtained through measurement [10]. In the context of an evolving emphasis on sustainable eco-friendly design, considerations extend beyond energy and environmental aspects to encompass human well-being [11]. Numerous green building certification systems have acknowledged this shift, incorporating evaluations of the light environment within indoor spaces as a certification criterion. Among these systems are LEED (Leadership in Energy and Environmental Design, USA), BREEAM (Building Research Establishment Environmental Assessment Method, UK), and DGNB (German Sustainable Building Council, Germany). Recent certifications, such as WELL and Fitwel, which underscore health and wellness, have also identified the lighting environment as a pivotal component. Notably, Korea's G-SEED (Green Standard for Energy and Environmental Design, Republic of Korea) evaluates the lighting environment in educational spaces but does not extend this evaluation to workspaces. The various certification systems that integrate daylighting evaluations have set specific criteria to foster suitable lighting conditions and minimize glare, which is a common issue for occupants of indoor spaces. These glare standards predominantly evaluate the integration of glare prevention mechanisms in artificial lighting or glare prevention systems based on daylight. To effectively design a glare prevention system influenced by natural lighting, it is crucial to anticipate how glare manifests within indoor spaces. During the design phase, such predictions are feasibly achievable primarily through simulations [9].

The primary objective of this study was to conduct a comparative analysis distinguishing between predicted glare levels derived from light environment simulations and actual measurements. The effective implementation of a system to mitigate glare caused by natural lighting necessitates a proactive approach to predicting how glare may manifest before constructing the space.

2. Materials and Methods

This study consisted of a comparative analysis between actual measurements and simulation results, specifically targeting glare. The methodology and process of this study were as follows (Figure 1):

1. A comprehensive review of previous studies was performed to clarify the characteristics and effects of artificial lighting and natural daylight, which collectively contribute to the composition of the light environment. Additionally, the underlying causes of natural daylight deficiency within office environments were identified, and the specific challenges that must be addressed to facilitate the integration of natural daylight indoors were highlighted.

2. In relation to the glare effect, which makes it difficult to introduce natural daylight indoors, the terminology and measurement methods related to glare were organized. A comparison was then made to assess how luminance (glare) was evaluated in green building certification systems, such as LEED, BREEAM, DGNB, WELL Certification, Fitwel Certification, and G-SEED. By reviewing these evaluation methods, the necessity of simulations to effectively prevent glare was examined. The research also verified the effectiveness of commonly used light environment simulations in optimizing lighting conditions in planning within actual construction environments. Based on the findings of this verification research, the need for further studies on simulation validation was confirmed.

3. To validate the simulations, actual measurements in real spaces were essential. Therefore, existing methods used for measuring space glare from previous studies were analyzed and compared with the measurement method employed in this study to identify its unique features and differentiating factors.

4. The research methodology for this study involved conducting actual measurements and simulations of luminance in three selected workspaces based on specific criteria. Actual measurements were carried out during two separate time slots, 2:00 PM and 4:00 PM, corresponding to the times when sunlight most significantly enters indoor spaces. Daylight glare probability (DGP) was chosen as the measurement metric

for comparison with the actual measurements. This choice was influenced by the widespread use and validation of the DGP for evaluating the probability of daylight-induced glare in spaces, following its proposal by Wienold and Christoffersen in 2006. To perform these simulations, ClimateStudio (Version 1.9) [12] was selected as the simulation program for the study due to its ability to measure glare based on DGP and its effective integration with Rhino, a popular architectural modeling tool.

5. Comparisons were made between the previously obtained actual measurement values and those generated from the simulation of the light environment. The results of these comparisons were then analyzed. This analysis aimed to identify the factors required to achieve more accurate predictions by simulations concerning light environments.
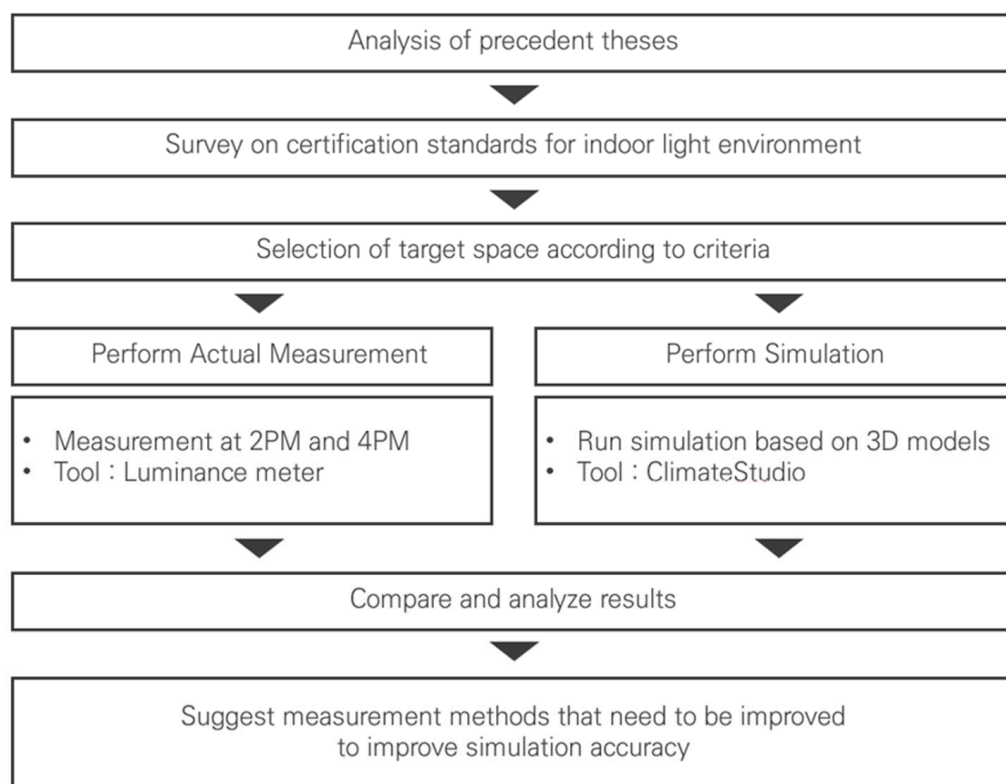

Figure 1. Research plan.

3. Previous Reviews

3.1. Characteristics and Effects of Daylight and Artificial Lighting

The light environment of an indoor space is composed of daylight and artificial lighting. These two sources have different characteristics and can affect occupants differently. First, artificial lighting has the advantage of ease in maintaining a uniform lighting environment, and its lighting properties, such as illuminance, color temperature, and color rendering, can be set in various ways. These features of artificial lighting enable a great deal of control over the light environment according to user needs, which can enhance efficiency by creating a suitable light environment for specific work activities. In contrast, in the case of daylight, it is difficult to maintain a constant light environment, as with artificial lighting, but it provides different advantages. The effective use of daylight can reduce dependence on artificial lighting, thereby reducing electric consumption. This leads to cost savings in building operations and enables environmentally friendly and sustainable building management [13]. Moreover, daylight improves the quality of the indoor environment and positively affects human health and comfort [14–17]. Illumination originating from sunlight can help regulate circadian rhythms and strengthen the immune system; it also allows for better psychological satisfaction and visual comfort in work or living environments [18–20].

Despite the numerous benefits of access to daylight in indoor spaces, many existing workplaces do not actively use it [21], because daylight's dynamic nature makes it difficult to control; furthermore, it could cause glare or hinder thermal comfort [22,23]. To minimize these negative effects while providing daylight in indoor spaces, it is necessary to consider how it will enter the space during the building design stage.

3.2. Glare-Related Terms and Metrics

Various methods are available for measuring the indoor lighting environment, with each green building certification system applying distinct metrics for its evaluation. Among the many light environment evaluation factors, emphasis is placed on defining and summarizing luminance and glare, which form the central point of this discussion.

First, luminance is a physical concept that represents the amount of light emitted or reflected from a specific surface or light source. The SI unit for luminance is candelas per square meter (cd/m^2). Luminance appears differently, depending on the angle between the glare source and the observer's line of sight. There are thresholds for perceived glare based on absolute luminance values and contrast thresholds based on differences in brightness between the glare source and background.

Regarding the luminance threshold according to absolute luminance values, Weinold and Christofferson [24] suggested that, when an occupant is positioned parallel to a window, glare is perceived as below 2000 cd/m^2, and visual discomfort is experienced as above 4000 cd/m^2. When an occupant looks at a window at a 45 degree angle, glare is perceived as below 1500 cd/m^2, and visual discomfort is experienced as above 4500 cd/m^2. Suk et al. [25] stated that, when looking vertically at a window, occupants feel visually comfortable with a luminance of 1920 cd/m^2 or below and experience visual discomfort with values above 5014 cd/m^2.

Regarding contrast thresholds based on brightness differences, Weinold and Christofferson [24] and Veitch and Newsham [26] argued that the upper limit of tolerable glare occurs when the contrast ratio between a glaring light source and its background reaches 1:10. Schiler [27] suggested that this threshold occurs when the ratio reaches 1:3 with respect to average ambient background levels, and Egan [28] proposed it happens with ratios of darkest-to-brightest sources reaching up to 1:40. These differing views arise because individual perceptions of glare vary by person and environment.

Second, glare is a visual impairment phenomenon that occurs when a high luminance source or large luminance contrast is presented in the field of view. It can occur when the iris reaction, which responds to changes in light, is delayed and cannot focus or when visual sensitivity is disrupted due to a scattering of light entering the eyeball. As previously explained, even with the same intensity and contrast of luminance, the degree of glare an individual perceives can vary. Although glare is not entirely quantifiable, typical evaluations are conducted in comfortable and uncomfortable light environments for specific environmental conditions.

Glare can be classified into disability glare and discomfort glare. Disability glare impairs the ability to visually perceive objects and often occurs to nighttime drivers. Discomfort glare does not impair visual perception but causes psychological discomfort and displeasure, such as eye fatigue. The way to measure and evaluate glare may vary according to the certification system; most evaluate glare caused by indoor artificial lighting, with the UGR (unified glare rating) being commonly used for evaluation. The UGR is a system for evaluating glare proposed by the CIE (International Commission on Illumination), mainly used for predicting indoor lighting systems. However, the current study conducted an evaluation of glare caused by daylight rather than artificial lighting. Thus, the DGP (daylight glare probability) was utilized as a system for evaluating glare, as it is especially applicable in scenarios with a wide range of light sources, including daylight.

The DGP has been widely used and validated for evaluating the probability of daylight-induced glares since it was proposed by Wienold and Christoffersen in 2006 [29]. ClimateStudio, a lighting environment analysis tool, incorporates DGP evaluations. It considers

multiple parameters, such as vertical illuminance at the observer's eye level (E_v), source luminance (L_s), the solid angle subtended by the source (ω_s), and the Guth position index (P) [30]. The value related to the probability occurrence of daylight-induced glares can be derived through calculation with the formula shown in Figure 2, which results in a value in the range of 0–100%. DGP values are divided into four bands according to their magnitude; higher values imply higher probabilities of occurrence.

$$DGP = c_1 \cdot E_v + c_2 \cdot log \left(1 + \sum \frac{L_{s,i}^2 \cdot \omega_{s,i}}{E_v^{a_1} \cdot P_i^2}\right) + c_3$$

E_v : Vertical eye illuminance in lx $\qquad$ L_s : Source luminance in cd/m²

ω_s : Solid angle of source $\qquad$ P : Position index

c_1 : $5.87 \cdot 10^{-5}$ $\qquad$ c_2 : $9.18 \cdot 10^{-2}$ $\qquad$ c_3 : 0.16 $\qquad$ a_1 : 1.87

Glare rating	DGP
Imperceptible	DGP ≤ 0.34%
Perceptible	34% < DGP ≤ 38%
Disturbing	38% < DGP ≤ 45%
Intolerable	45% < DGP

Figure 2. Calculation formula and glare rating of the DGP.

3.3. Glare Evaluation Method by Certification System

The evaluation of the visual environment in LEED is divided into Interior Lighting, Daylight, and Quality Views. Among them, glare is evaluated in the interior lighting area, along with color rendering, lighting control, and surface reflectance. In this area, one point is given if one out of four items is satisfied, and two points are awarded if three items are met. To meet the glare control item requirement, the luminance of indoor lighting fixtures must be less than 7000 cd/m² or have a UGR rating of less than 19.

BREEAM evaluates the visual environment based on Control of Glare, Daylighting, View Out, and Lighting Levels/Zoning/Control. The evaluation of glare control assesses potential glare occurrence in indoor spaces and whether measures such as shading have been established for control. These mitigation strategies should aim to maximize daylight use without increasing energy consumption from lighting under all weather conditions.

DGNB evaluates the visual environment based on Daylight, Visual Contact, Antiglare, Artificial Light, and Color Rendering. Among these categories, a glare prevention assessment depends on whether a system has been installed to prevent glare caused by daylight and grades the system accordingly. When a building incorporates both solar protection systems and glare prevention systems, the evaluation is conducted based on the higher-rated system of the two.

LEED, BREEAM, and DGNB are early certification systems that emerged alongside discussions about eco-friendly architecture and continue to be revised, reflecting the current needs. While initial certification systems began with evaluations from an energy and environmental perspective, they now also incorporate assessments from an occupant well-being perspective. However, the tendency toward evaluation from an energy and environmental perspective remains stronger. Compared to the three aforementioned certifications, WELL and Fitwel are relatively recently established and place stronger emphasis on the environment's impact on occupant well-being and health in their evaluations. Although there are

differences in overall trends between certification systems, WELL is similar to LEED and Fitwell is similar to BREEAM and DGNB in terms of evaluating glare.

In WELL certification, the visual environment evaluation consists of nine categories: (1) Light Exposure, (2) Visual Lighting Design, (3) Circadian Lighting Design, (4) Electric Light Glare Control, (5) Daylight Design Strategies, (6) Daylight Simulation, (7) Visual Balance, (8) Electric Light Quality, and (9) Lighting Control. The glare control category is intended to prevent glare caused by indoor lighting, and it assesses the glare index associated with indoor lighting. To satisfy antiglare control requirements, indoor luminosity fixtures must have luminance less than 6000 cd/m^2 or an UGR rating less than 16.

Fitwel certification evaluates Daylight, View of Nature, and Operable Shading in regard to the light environment within workspaces. Operable shading is an evaluation factor for glare prevention. For spaces designated as general occupancy areas, all windows should be equipped with shades that can be controlled by the occupants.

G-SEED evaluates the presence of shading as a factor in glare assessment. However, this evaluation is conducted only for educational facilities and not office buildings.

The aforementioned certification systems adopt UGR in their glare evaluation systems. While this is a suitable criterion for assessing indoor lighting, it is not an appropriate system for evaluating glare caused by natural daylight. In cases where there are measures to control glare induced by natural daylight, most evaluations primarily focus on verifying the presence of glare prevention systems. The evaluation schemes for all the certification systems described are summarized in Table 1.

Table 1. Glare evaluations of the certification schemes.

Certification	Workspace Evaluation	Glare Evaluation Method			Score
LEED	O	Interior Lighting	Glare Control	<7000 cd/m^2 or UGR < 19	1~2 *
			Color Rendering	RA $\geq$ 90	
			Lighting Control	Brightness Control of Lighting (90% of exclusive area)	
			Surface Reflectance	Ceiling $\geq$ 80%	
				Wall $\geq$ 55%	
BREEAM	O	Control of Glare		Glare Prevention Strategy (There should be no increase in lighting energy usage)	1
DGNB	O	Antiglare		Installation of Glare Prevention System	8
			Glare Prevention System Grade	=Grade 1	12
				$\geq$Grade 2	16
WELL	O	Electric Light Glare Control		<6000 cd/m^2 or UGR $\leq$ 16	2
Fitwel	O	Operable Shading		Installation of Operable Shading	0.28
G-SEED	X	Antiglare		Installation of Shading (Educational Facilities)	2

* Satisfying one of the detailed evaluation items: 1 point. Satisfying three of the detailed evaluation items: 2 points.

3.4. Distinction from Previous Studies

From the literature retrieved from SCOPUS using the keywords "simulation" and "glare", Diva and ClimateStudio (formerly referred to as DIVA-for-Rhino) were found to be the major analysis tools. Additionally, it was confirmed that the DGP method was frequently used. Moreover, most of the studies using DIVA or ClimateStudio for glare analysis appeared to utilize simulations to predict and optimize lighting conditions [31–59]. However, none of these studies addressed ways to improve the potential limitations of these simulations.

This study investigated the lighting environment in workspaces subject to glare caused by daylight using both actual measurements and simulations. Through a comparison of these results, we sought to identify and discuss elements that deserve further consideration in lighting environment simulations.

The high dynamic range (HDR) image creation method is commonly used for measuring a lighting environment's luminance and illuminance [60,61]. This method involves capturing a scene in space with a fisheye lens and digital camera, measuring the luminance at one point in that scene with a luminance meter and applying the obtained value as a correction to the image. When luminance measurements are conducted using the HDR method, the luminance of all images captured within the fisheye lens is measured.

However, according to Safranek [62], the HDR method has errors due to lens vignetting, lens flare, sensor blooming/luminous overflow, and the spectral responsivity of the sensors. Furthermore, in the current study, because only glare caused by daylight is considered, it was deemed inappropriate to use the HDR method for actual occupied workspaces, as they could be influenced by the luminance of artificial lighting and digital devices.

To mitigate potential errors associated with the HDR method and to exclude the influence of artificial lighting, this study utilized a luminance meter (CS-150, Konica Minolta) that measured the luminance at localized points (measuring angle 1°) (see Figure 3). Luminance measurements were conducted in the direction of the windows, where luminance from natural daylight was anticipated. As depicted in Figure 3, the luminance measurement was carried out in an environment illuminated by both natural and artificial light sources. However, since the measurement specifically targeted a window receiving natural light, the impact of artificial lighting on the recorded luminance value was minimal.
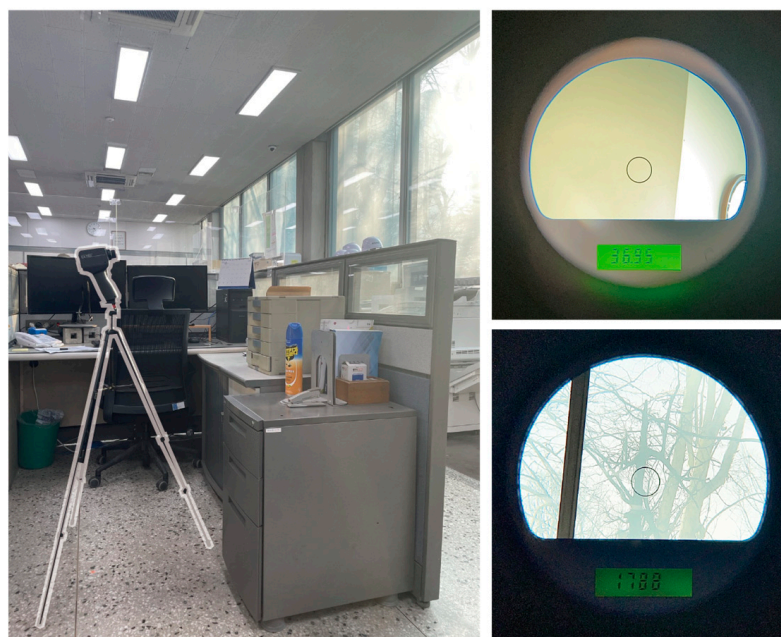
Figure 3. Luminance meter installation and viewport.

4. Experimental Space and Methodology

4.1. Space Selection and Criteria

In comparing the actual measurements to the simulation results, the Offices of Academic Affairs, Administration, and Industry-Academic Cooperation at Hongik University (Seoul, Republic of Korea, 37°33′02.6″ N 126°55′33.5″ E) were designated as the focal spaces. All three offices were situated in the MH Building on campus. The criteria for choosing buildings for the light environment assessment were accessibility for research measurements and unobstructed natural light ingress devoid of interference from nearby

structures or installations. Given these criteria, the MH Building was selected from among the accessible campus buildings; due to its elevated location, it ensured unhindered natural light during the study. The building's substantial size, spanning 16 stories, further influenced our choice given the diversity of spaces it offered. Within the MH Building, our chosen spaces took into account a mix of attributes, such as size, floor level, geographical position, and altitude, ensuring a variety of characteristics (Table 2).

Table 2. Characteristics of each target space.

Space	Characteristics				
	Floor	**Altitude**	**Area**	**Floor Height**	**Location**
A	1F	1.05 m	129 m^2	4.08 m and 2.3 m	North of MH Building
B	8F	26.6 m	102 m^2	2.8 m	Center of MH Building
C	1F	1.05 m	153 m^2	4.08 m and 2.3 m	South of MH Building

The Office of Academic Affairs (Space A) was located on the first floor to the north, with windows facing west (Figure 4). The Industry-Academic Cooperation Foundation Office (Space B) was located on the 8th floor, with windows on three sides (none to the east). The Office of General Affairs (Space C) was located on the first floor to the south, with windows facing west. Measurement points were arranged at 2 m × 2 m intervals in each space, depending on each space's unit area. There were 40 measurement points in Space A, 27 in Space B, and 40 in Space C (Figure 5).
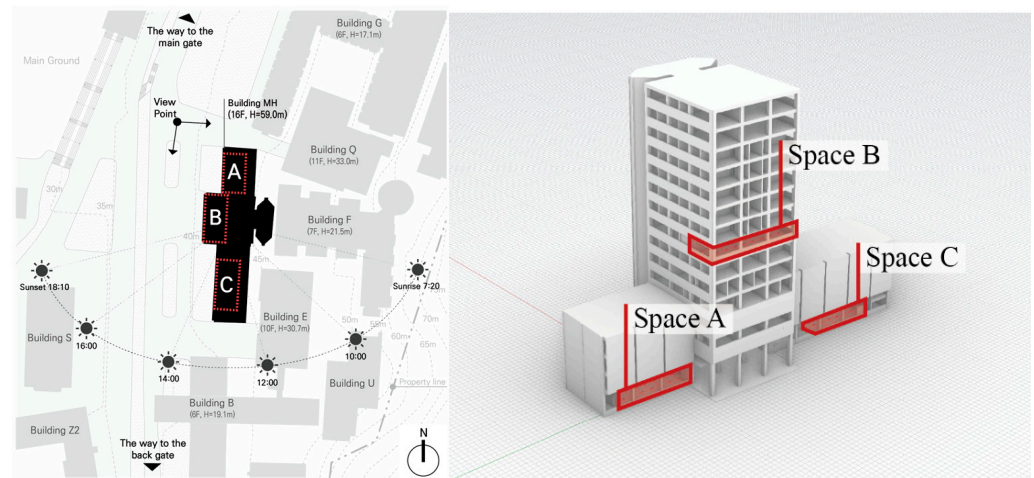
Figure 4. Site plan and positions of the target spaces.
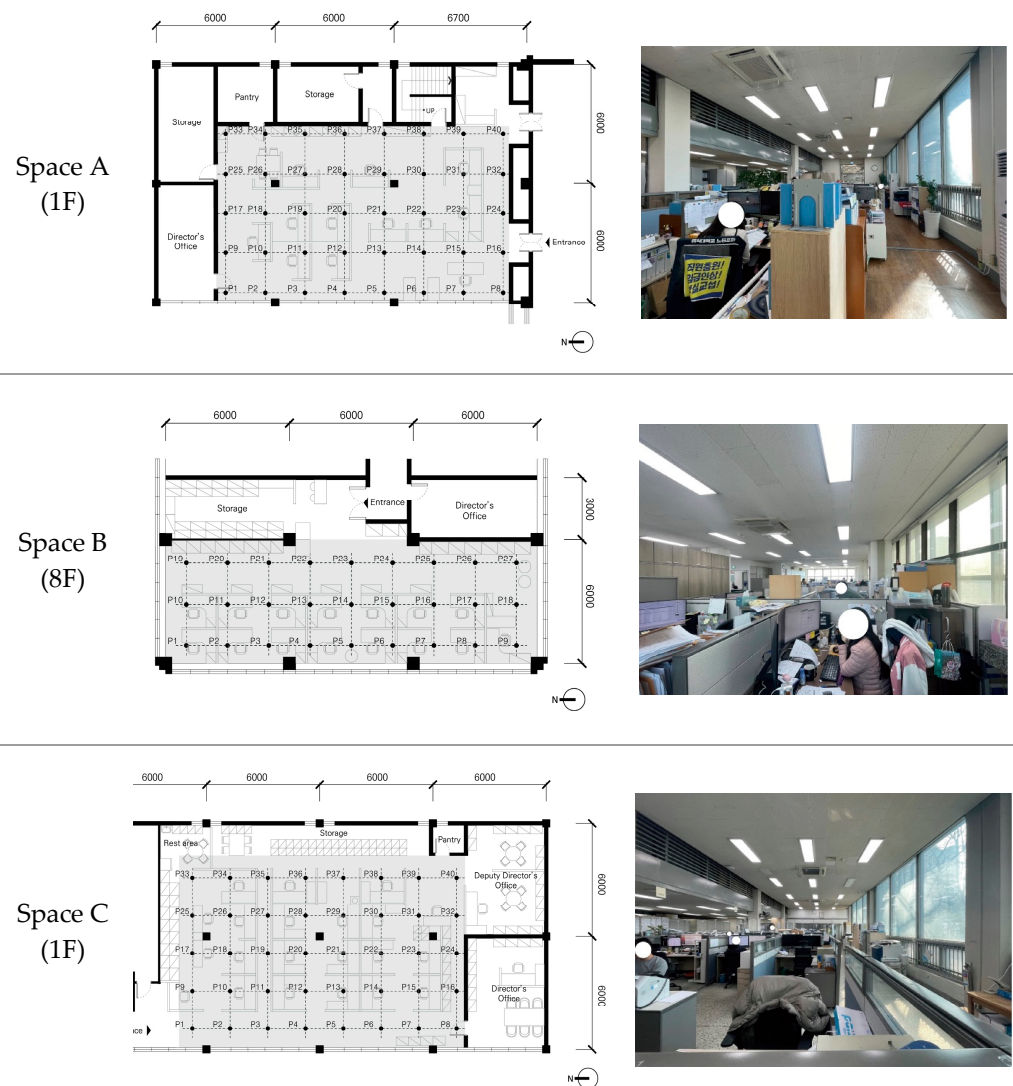
Figure 5. Floor plans and measurement points (**left**), and photographs of the target spaces (**right**).

4.2. Method for Luminance Measurement Using a Luminance Meter

In this study, we aimed to measure the occurrence of glare caused by daylight. Consequently, we planned to measure the luminance in the direction of the windows, where most of the glare was expected due to daylight. For the target spaces, as visual openness through the windows primarily faced west, measurements were conducted in three directions: northwest, west, and southwest. The interval between each measurement point was set at 2 m × 2 m (Figure 6).
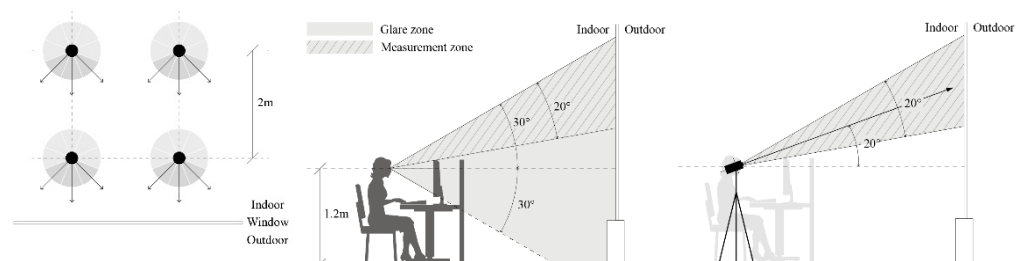
Figure 6. Measurement points and directions (**left**), glare zone (**center**), and measurement settings (**right**).

To enhance the accuracy of the luminance measurements, specific points were pre-marked on the floor of the measurement space. Additionally, to ensure consistent vertical and horizontal angles during the luminance readings, corresponding angles were indicated on the tripod that held the luminance meter. This process aimed to mitigate potential discrepancies during each measurement. However, minor errors might have been introduced due to the physical process of initiating each measurement, a common challenge with manual experimental readings.

When scheduling the actual measurements, shading effects from the exterior landscaping on Spaces A and C had to be considered, given their locations on the lower floors. As a solution, readings were conducted during the winter months, specifically from 21 to 23 February 2023. The measurements for Space A (1F) took place on 21 February, Space B (8F) on 22 February, and Space C (1F) on 23 February. While this timing presented a limitation in observing luminance variations that might occur in other seasons, it provided a more controlled environment. This control facilitated a focus on differences stemming solely from natural lighting rather than other environmental factors.

Regarding the specific times for measurements, the readings were segmented into two slots: 2:00 PM, when the onset of direct natural light into the west-facing areas was anticipated, and 4:00 PM, when a more profound penetration of natural light into these spaces was expected. A broader time range for the measurements was not feasible, because the spaces were operational work areas.

In the case of the actual physical measurements using a luminance meter, there were multiple measurement points and directions, so there were limitations in measuring the light environment at exactly the same time for each measurement point. Therefore, in this experiment, luminance measurements were carried out over a period of time that included the exact simulation time: from 2:00 to 2:50 PM and from 4:00 to 4:50 PM. A CS-150 luminance meter (Figure 7), manufactured by Konica Minolta (Tokyo, Japan) [63], was employed for these measurements. This device is widely utilized to assess luminance in diverse applications, including displays, LEDs, outdoor and indoor lighting fixtures, diverse light sources, and various other lighting setups. In this experiment, it was employed to gauge the luminance generated by daylight in a workspace. On all three measurement days, the weather conditions in Seoul were clear, with cloud coverage between zero and two-tenths [64]. The external illuminance measured using a Konica Minolta CL-500a spectroradiometer (Figure 7) during each time slot is shown in Table 3 [65].

Figure 7. Luminance meter (**left**) and illuminance meter (**right**).

Table 3. Measurements of external illuminance (Unit: lx).

Time	Day		
	21 February 2023	22 February 2023	23 February 2023
2:00 PM	70,310	68,006	60,840
4:00 PM	33,147	24,886	27,247

Traditional methods of measuring glare typically involve the use of HDR imaging with a fisheye lens to set the measurement range at 180 degrees. However, according

to the research by Suk et al. [66], the field of view (FOV) of the human vision system is smaller than that of a fisheye FOV. In their study, it was found that, during typing tasks, the human vision system's FOV accurately detected 97% of glare sources, while the fisheye FOV accurately detected only 55% of glare sources in a scene. Consequently, they argued for using the human vision system's FOV when evaluating scenes for glare.

The human eye contains photoreceptor cells, described as cones and rods. Cones function well under high illumination levels during daylight and are responsible for color discrimination; rods function well at low illumination levels at night and distinguish shades of gray. These photoreceptor cells are differentially distributed across the retina: cones exist at a low density across most of the retina but are denser toward the fovea (the center), while rods are densely packed throughout most parts of the retina but dramatically decrease in density near the fovea [67]. This distribution corresponds with suggestions that humans perceive light and color better within approximately 30 degrees centered on their line of sight.

In this research, we therefore defined an angle within 30 degrees from one's gaze as our "glare zone". Given that our target space was used as an office space with furniture arrangements potentially obscuring some areas from view, we excluded these obscured regions from our measurements. We assumed that any glare caused by daylight would occur 10–30 degrees above one's line of sight (Figure 6). Accordingly, we set up our luminance meter to measure luminance centered on an angle 20 degrees above a typical individual's line of sight.

4.3. Method for Glare Measurement Using Simulation

For the simulations, this study used ClimateStudio (Version 1.9), a plug-in program developed by Solemma that can be used in conjunction with Rhino, a 3D modeling program developed by Robert McNeel. Therefore, Rhino 7 (Version 7.13) was used to create 3D models for the simulation. The floor plans and elevations of Spaces A, B, and C were used to create the 3D models. For the actual spaces, the ceiling was made of white textile with a reflectance of 50–70%, the walls were covered by a light cream color paint with about 50–60% reflectance, and the floor was composed of materials with a reflectance of 20–30%. The windows were double-glazed and had a very slight tint, possessing performance values similar to the visible transmittance (VTIS) applied in the simulation. The VTIS is a value that affects the amount of light entering indoors. A similar VTIS value in the actual space and the simulation space implies that a similar amount of light entered both indoor environments. Because the materials applied in the actual space had properties similar to those recommended by the LEED standard, all spatial elements in the 3D model were applied with materials recommended by the LEED standard (Figure 8). After assigning materials according to the architectural elements, we set up location-specific climate data. The climate data utilized were an energy plus weather format (EPW) file provided by Energy Plus, an energy simulation program developed by the U.S. Department of Energy (DoE). Among the EPW files available, we used KOR_SO_Seoul.471080_TRY_PHIKO.epw, which was based on weather data measured by the Korea Meteorological Administration in Seoul. The sky settings were configured within ClimateStudio to match the sky conditions on the days when the actual measurements were taken—the CIE Standard Clear Sky setting was used in this case. Based on this, an annual glare analysis was conducted in ClimateStudio, targeting the created 3D model. From the results obtained through the simulation analysis, only the data from the same date as the actual measurements were extracted for comparison. Because the simulation provided glare values at 30 min intervals, the DGP values extracted at 2:30 PM and 4:30 PM were used for comparison. Furthermore, measurement points were spaced at intervals of 2 m × 2 m and were aligned to correspond with the actual measurement locations. The direction of measurement in the simulation was also aligned in the same direction as the actual measurements.

Window: *Solexia-Solaban 60*

U-value=1.66

Solar heat gain coefficient (SHGC) =0.368

Visible transmittance (TVIS) value=0.610

Double-glazing with a thickness of 24.1mm

Ceiling: *Ceiling IES LM-83*

Diffusion rate = 70%

Reflectance = 70%

Floor: *Floor IES LM-83*

Diffusion rate = 20%

Reflectance = 20%

Wall: *Wall IES LM-83*

Diffusion rate = 50%

Reflectance = 50%

Analysis Surface(h=1.2m)
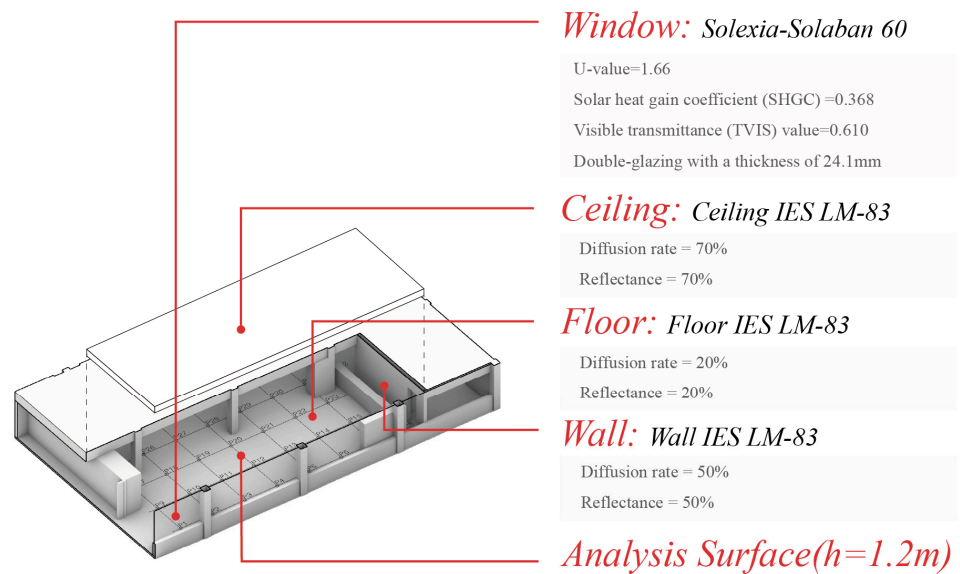
Figure 8. Three-dimensional model for simulation.

5. Results: Comparison of Simulation and Actual Measurements

5.1. Space A

　　Space A (Figure 9; additional details in Appendix A) had windows located on the west side, with the floor height of the space where the measurement points P1–P24 were located being 4.05 m, and the space where P25–P40 were located had a lower floor height of 2.3 m. The windows started at 0.85 m above the floor and reached the ceiling, with a total height of 3.2 m. At approximately 2:00 PM, sunlight did not directly enter the field of view in Space A. On 21 February, at 2:00 PM, the sun's position was at an azimuth of 203 degrees and an elevation angle of 38 degrees, passing the meridian. Consequently, in the absence of any external obstructions, sunlight should have been visible in west-facing Space A. However, Space A did not receive direct sunlight, because it was blocked by a midsection of the MH Building protruding about six meters to the west.
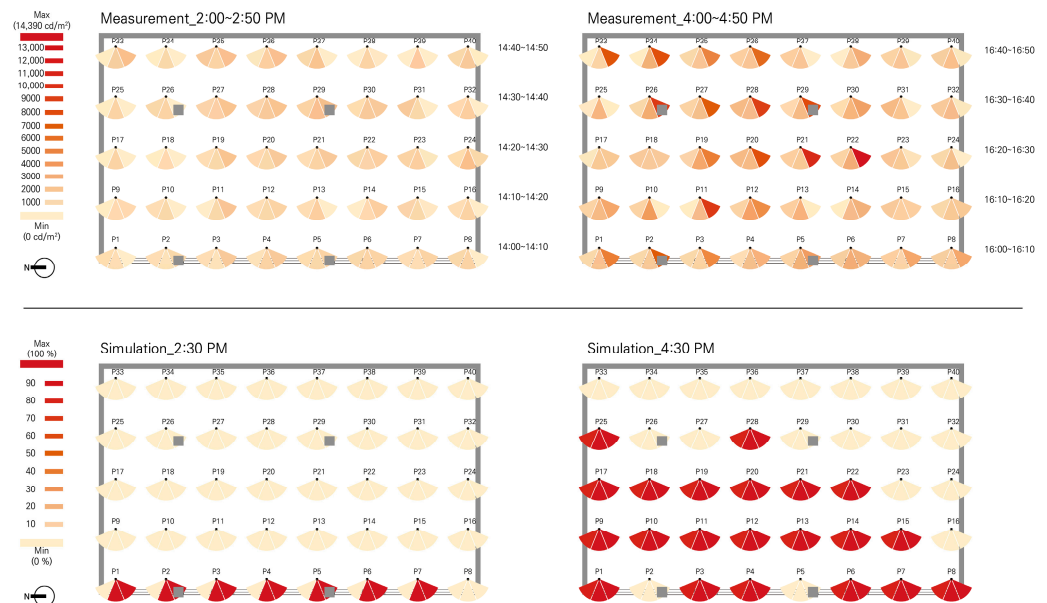
Figure 9. The measurement and simulation results of Space A (The gray box area in this Figure is the same as the gray area in Figure 5 above, which indicates the measurement area. Detailed data are included in Appendix A).

The results of the luminance measurements conducted on Space A showed that, at 2:00 PM, there was no influx of direct sunlight; hence, no points within the space exhibited especially high values. However, it was observed that, generally, higher luminance values were recorded when measurements were taken in the southwest direction. This trend became more pronounced around 4:00 PM as direct sunlight began to enter the space. The luminance values measured in the southwest direction showed significantly higher figures, and with each 45 degree rotation of the measurement direction toward the north, there was a marked decrease in these values.

The simulation results for Space A revealed that, at 2:30 PM, only the positions P1~P7 located near the window exhibited a DGP value of 100% in the southwest and west directions. Other measurement points showed almost negligible DGP values at this time, registering at 0.3%. At 4:30 PM, as the sun moved farther west and its altitude decreased, there was an increase in locations within the space experiencing glare. At these glare occurrence points, the DGP values were recorded as 80% in the northwest direction and consistently 100% in both the southward and westward directions. In other areas during this time frame, the DGP was virtually nonexistent, with a value of 0.3%.

5.2. Space B

Space B (Figure 10; additional details in Appendix B) was the only space among the target areas that had windows facing the south, west, and north. The floor height in Space B was uniformly set at 2.8 m throughout, with no variation. The windows began 1.1 m above the floor and reached the ceiling, with a total window height of 1.7 m. In the case of Space B, due to its lower ceiling height compared to Spaces A and C, there were occasions where the luminance of the ceiling was mistakenly measured instead of the window luminance when measurements were made 20 degrees upward for points P19–P27, which were farthest from the window. However, according to the actual measurement data at 4:00 PM in this experiment, there was still a spot showing strong luminance at that location. This may have been due to the refraction of light by the window and the reflection of light by the ceiling, as these measurement points were close to the window edge.

Figure 10. The measurement and simulation results of Space B (The gray box area in this Figure is the same as the gray area in Figure 5 above, which indicates the measurement area. Detailed data are included in Appendix B).

Unlike Spaces A and C, Space B had windows facing south, west, and north. Therefore, it was anticipated that Space B would exhibit stronger luminance compared to the other two spaces.

However, the actual luminance measurements in Space B did not identify any points with higher luminance values compared to the other spaces. This could be due to the fact

that the measurement points for luminance were taken pointing upwards at a 20 degree angle from a typical observer's eye level (1.2 m), and at around 2:00 PM on 22 February, the sun's altitude was 39 degrees, located higher than this viewing angle. By around 4:00 PM, the sun's altitude dropped to about 24 degrees, which aligned closely with the luminance meter's measurement angle. At this time, the sun's azimuth angle was approximately 233 degrees, which was close to directly southwest. Therefore, high luminance values were observed when measurements were taken in the southwest direction.

The simulation results for Space B revealed that, at 2:30 PM, glare with a DGP of 100% was predicted to occur in the west and southwest directions from positions P9, P18, and P27 located near the south-facing windows. In the other locations, the DGP value was observed to be nearly negligible at 0.3%. By 4:30 PM, glare was detected not only at the south-facing window positions but also at those facing west. The DGP values for both the southwest and west directions were found to be 100% at the points where glare occurred, while it was in the range of 79–82% only in the northwest direction. The innermost locations within the space, specifically P19–P26, exhibited almost no occurrence of glare, with a DGP of 0.3%.

5.3. Space C

Like Space A, Space C (Figure 11; additional details in Appendix C) had windows facing west. However, it distinguished itself from Space A in that there were no buildings obstructing the influx of sunlight during the afternoon hours. The ceiling height of the space where the measurement points P1–P24 were located was 4.05 m, identical to that of Space A, and the area where P25–P40 were located also had a ceiling height of 2.3 m. The windows began 0.85 m above the floor and reached the ceiling, with a total height of 3.2 m. On 23 February, when the measurements for Space C were conducted, at 2:00 PM, the sun's azimuth was 203 degrees, and its altitude was 39 degrees; at 4:00 PM, its azimuth was 234 degrees, with an altitude also at 39 degrees.
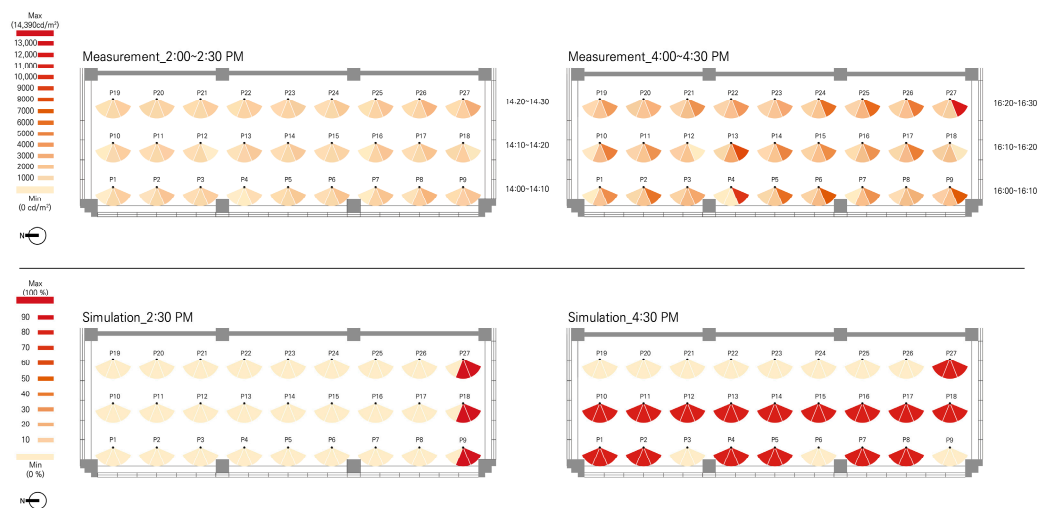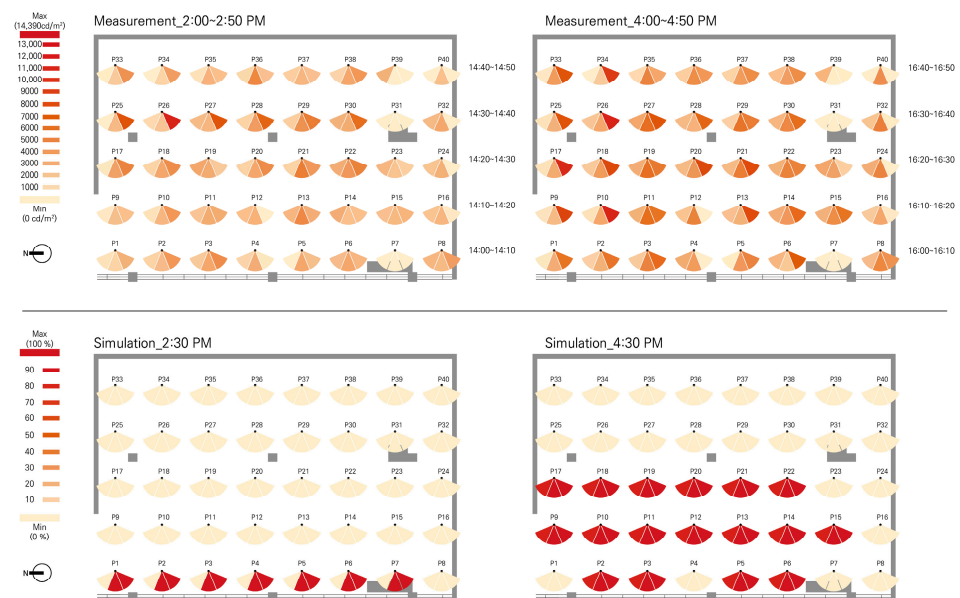

Figure 11. Measurement and simulation results of Space C (The gray box area in this Figure is the same as the gray area in Figure 5 above, which indicates the measurement area. Detailed data are included in Appendix C).

Similar to the other areas, the luminance data measured around 2:00 PM did not show significant variations among the different points and directions. However, around 4:00 PM, as more light entered the space due to the lower solar altitude, noticeable differences in the luminance values were observed among the various points and directions.

The simulation results for Space C indicated that, at 2:30 PM, only the positions P1–P7 located near the west-facing window exhibited a DGP value of 100% in the southwest and

west directions. In other locations, the DGP value was approximately 0.3%, indicating almost no occurrence of glare. At 4:30 PM, as the sun's altitude decreased, allowing more sunlight to enter the interior, there was an increase in the locations experiencing glare. However, measurement points P23–P40, located in areas with lower ceilings, showed almost no occurrence of glare (DGP values about 0.3%). Measurement points located at a higher floor height generally showed a high probability of glare occurrence. At the point where glare occurred, the DGP values were 100% in both the southwest and west directions and 83% in the northwest direction.

6. Discussion

Upon comparing the results of the field measurements and the simulations for Spaces A, B, and C, it was observed that both the actual measurement and simulation confirmed more glare occurrence between 4:00 PM and 4:50 PM than between 2:00 PM and 2:50 PM. Although the external illuminance measured earlier (Table 3) showed stronger illuminance at 2:00 PM than at 4:00 PM, the glare inside the space appeared stronger around 4:00 PM when the sun's altitude was lower. This suggests that glare was more influenced by the presence or absence of direct sunlight entering a space due to changes in the solar altitude and azimuth angle rather than by external illuminance.

Between 2:00 PM and 2:50 PM, although luminance changes occurred according to the direction of the field measurements, all values (except those from P2, P3, P10, P13, P17, P18, P20, P21, P22, P28, P29, P33, and P38) in Space C measured below 4000 cd/m^2. Therefore, according to the standards suggested by Weinold and Christofferson [19], almost no locations in Spaces A and B would cause visual discomfort for individuals due to glare. Nevertheless, the simulation predicted that, in all the spaces (Spaces A, B, and C), the DGP values would reach 100 at measurement points near the windows, signifying the occurrence of glare. This highlights an inconsistency between the actual measurements and the simulation results. For the more effective use of simulations in light environment planning, understanding and addressing the sources of this discrepancy in the simulation is essential.

For the period between 4:00 PM and 4:50 PM, the field measurements showed stronger variations in luminance depending on the direction and a significant increase in points where the luminance was high enough to cause visual discomfort. During the same time period, the simulation also predicted an increase in locations likely to experience glare. Notably, in the field measurements, there were no instances of strong luminance causing discomfort in the northwest direction. However, the stimulations identified numerous points with DGP values of approximately 80% in this direction. In addition, concerning the actual measurements, elevated luminance values capable of causing discomfort were observed, even in areas relatively far from the windows. Conversely, the simulations showed that, in the innermost parts of the space, the DGP values were almost negligible at 0.3%.

The prediction of strong luminance occurrence in the northwest direction through simulations can be attributed to differences arising due to the light collection method used for the DGP calculation. This method employed fisheye rendering techniques to collect light sources within a 180 degree angle, which may have resulted in disparities based on light information collection and associated computation methods. The glare analysis using fisheye rendering in the simulation is based on the same principle as the HDR method with a fisheye lens, a technique commonly employed in actual glare measurements. However, when the results of luminance measurements and simulations from this research were compared, there were instances where the simulation predicted high glare from directions not evident in the actual measurements. This discrepancy suggests that the simulation may have used an overly broad light capture range. Given that the human field of view (FOV) is more limited than that of a fisheye lens, using fisheye rendering to predict glare might lead to overestimations of glare compared to human perceptions. This could introduce inaccuracies in the simulation's predictions due to its light capture and analysis methods.

Therefore, to enhance the accuracy of the simulation, further investigation is needed on glare analysis methods using a human field of view (FOV) that considers the subjective feedback of occupants.

Concerning obstructions within spaces, for Spaces A and C, columns present within the measurement areas were accounted for in both the actual measurements and the simulation. For Spaces A, B, and C, the studies were designed to ensure that indoor furniture would not influence either the real measurements or simulation outcomes, resulting in negligible deviations due to furniture placement. Conversely, the effects of building columns were factored in, leading to instances in both the actual measurements and simulations in which the luminance readings were lower due to column obstructions. A summary of the comparisons is presented in Table 4.

Table 4. Comparisons of the actual measurements and simulation.

	Actual Measurement	Simulation
2:00 PM to 2:50 PM	- Except for some points in Space C, there were no areas exceeding 4000 cd/m^2.	- Glare was predicted to occur at window-side locations in Spaces A, B, and C.
4:00 PM to 4:50 PM	- Numerous points with luminance exceeding 4000 cd/m^2 were detected in Spaces A, B, and C. - Points with luminance exceeding 4000 cd/m^2 were also detected in the innermost part of the space. - There was a tendency for a significant difference in luminance to occur between the NW, W, and SW.	- It was predicted that glare would not occur in the innermost part of the space. - There was no significant glare difference between the NW, W, and SW.

7. Conclusions

While natural lighting offers numerous benefits, many workspaces resort to covering windows with blinds to mitigate glare. This approach not only obstructs external views but also reduces the influx of natural light. Therefore, architectural designs and placements that balance external views, natural light, and glare prevention are crucial. Simulations can be instrumental in light environment design. However, this study unveiled discrepancies between existing simulation results and actual measurements, possibly because the simulations employed fisheye rendering. Suk et al. [66] highlighted that a human's field of view (FOV) is narrower than that of a fisheye lens, leading to potential inaccuracies in glare capture. To enhance indoor glare assessments, simulations should incorporate a human FOV to discern glare variations by direction. Furthermore, beyond just the ClimateStudio program used in this research, a comparative analysis of various simulation tools is essential for refining the lighting environment.

The limitations of this study include the inability to perfectly replicate identical environments, minor measurement errors (such as those arising from the physical act of taking measurements) during data collection, and the incomplete removal of the shading effects of tree branches (despite conducting the experiments in winter to reduce these influences). Additionally, the simulations might have missed some temporary glare effects, because they predicted only specific time points. However, even with these challenges, consistent discrepancies were observed between the actual measurements and the simulation results, particularly in terms of the measurement direction and points. These differences suggest that the primary cause may not be factors such as external landscaping or unpredicted temporary glare effects in the simulations but, rather, a more significant factor, such as the light capture method in the simulations using the fisheye FOV.

For future research involving luminance measurements, it is imperative to develop a glare measurement method tailored to the specific environmental conditions of the chosen study space, such as partitions, occupants' eye level, and spatial depth. The glare zone defined in this research was specifically designed for the selected space. Moreover, to grasp

the variability of the data across time and space, further research should be conducted in environments and at times different from those in this experiment.

Appendix A

Table A1. Comparison of the luminance measurements and DGP simulations in Space A. Unit: cd/m^2 (measurement) and DGP (%) (simulation).

	Point		Measurement	Simulation	Point		Measurement	Simulation		Point		Measurement	Simulation	Point		Measurement	Simulation
2:00 ~ 2:30 PM	P1	NW	914	0.3	P21	NW	840	0.3	4:00 ~ 4:30 PM	P1	NW	1100	* 81.8	P21	NW	1518	* 81.8
		W	876	* 100.0		W	1321	0.3			W	2180	* 100.0		W	1900	* 100.0
		SW	44	* 100.0		SW	1778	0.3			SW	5576	* 100.0		SW	* 11,150	* 100.0
	P2	NW	847	0.3	P22	NW	1097	0.3		P2	NW	1200	0.3	P22	NW	1420	* 81.8
		W	686	* 100.0		W	1244	0.3			W	1900	0.3		W	3117	* 100.0
		SW	1120	* 100.0		SW	1594	0.3			SW	7365	0.3		SW	* 14,390	* 100.0
	P3	NW	870	0.3	P23	NW	1310	0.3		P3	NW	1164	* 81.8	P23	NW	2001	0.3
		W	561	* 100.0		W	1571	0.3			W	1427	* 100.0		W	1909	0.3
		SW	1761	* 100.0		SW	355	0.3			SW	5023	* 100.0		SW	565	0.3
	P4	NW	698	0.3	P24	NW	974	0.3		P4	NW	846	* 81.8	P24	NW	1114	0.3
		W	1367	* 100.0		W	2275	0.3			W	2349	* 100.0		W	2309	0.3
		SW	1736	* 100.0		SW	71	0.3			SW	2908	* 100.0		SW	93	0.3
	P5	NW	968	0.3	P25	NW	145	0.3		P5	NW	1410	0.3	P25	NW	264	* 81.8
		W	1183	* 100.0		W	1319	0.3			W	2994	0.3		W	2659	* 100.0
		SW	1288	* 100.0		SW	116	0.3			SW	3933	0.3		SW	172	* 100.0
	P6	NW	1200	0.3	P26	NW	1203	0.3		P6	NW	1605	* 81.8	P26	NW	1147	0.3
		W	1380	* 100.0		W	1467	0.3			W	3115	* 100.0		W	3221	0.3
		SW	1350	* 100.0		SW	118	0.3			SW	2954	* 100.0		SW	* 9727	0.3
	P7	NW	896	0.3	P27	NW	1266	0.3		P7	NW	1490	* 81.8	P27	NW	1354	0.3
		W	850	* 100.0		W	1839	0.3			W	1270	* 100.0		W	2357	0.3
		SW	1376	* 100.0		SW	2021	0.3			SW	3590	* 100.0		SW	* 7486	0.3
	P8	NW	1192	0.3	P28	NW	1257	0.3		P8	NW	1546	* 81.8	P28	NW	2464	* 81.8
		W	1294	0.3		W	1767	0.3			W	1672	* 100.0		W	2442	* 100.0
		SW	35	0.3		SW	2094	0.3			SW	282	* 100.0		SW	* 9290	* 100.0

Table A1. *Cont.*

	Point	Measurement		Simulation	Point	Measurement		Simulation		Point	Measurement		Simulation	Point	Measurement		Simulation
2:00 ~ 2:30 PM	P9	NW	201	0.3	P29	NW	1367	0.3	4:00 ~ 4:30 PM	P9	NW	1405	* 81.8	P29	NW	1051	0.3
		W	1009	0.3		W	2245	0.3			W	2605	* 100.0		W	2589	0.3
		SW	1047	0.3		SW	2336	0.3			SW	3513	* 100.0		SW	* 8576	0.3
	P10	NW	785	0.3	P30	NW	902	0.3		P10	NW	1339	* 81.8	P30	NW	966	0.3
		W	1172	0.3		W	1764	0.3			W	* 4035	* 100.0		W	2886	0.3
		SW	102	0.3		SW	1778	0.3			SW	228	* 100.0		SW	3753	0.3
	P11	NW	114	0.3	P31	NW	1712	0.3		P11	NW	243	* 81.8	P31	NW	2566	0.3
		W	1154	0.3		W	1170	0.3			W	2440	* 100.0		W	2088	0.3
		SW	2015	0.3		SW	48	0.3			SW	* 9725	* 100.0		SW	52	0.3
	P12	NW	816	0.3	P32	NW	1064	0.3		P12	NW	1347	* 81.8	P32	NW	1796	0.3
		W	1175	0.3		W	1668	0.3			W	3636	* 100.0		W	2444	0.3
		SW	1378	0.3		SW	39	0.3			SW	* 4815	* 100.0		SW	385	0.3
	P13	NW	837	0.3	P33	NW	142	0.3		P13	NW	1590	* 81.8	P33	NW	157	0.3
		W	1648	0.3		W	1547	0.3			W	2929	* 100.0		W	1347	0.3
		SW	97	0.3		SW	2289	0.3			SW	219	* 100.0		SW	* 7778	0.3
	P14	NW	102	0.3	P34	NW	153	0.3		P14	NW	152	* 81.8	P34	NW	170	0.3
		W	1060	0.3		W	1122	0.3			W	2443	* 100.0		W	3007	0.3
		SW	1667	0.3		SW	81	0.3			SW	2959	* 100.0		SW	* 8230	0.3
	P15	NW	1251	0.3	P35	NW	1787	0.3		P15	NW	1757	* 81.8	P35	NW	1127	0.3
		W	1104	0.3		W	1308	0.3			W	1511	* 100.0		W	1922	0.3
		SW	280	0.3		SW	2244	0.3			SW	658	* 100.0		SW	* 5202	0.3
	P16	NW	847	0.3	P36	NW	462	0.3		P16	NW	1149	0.3	P36	NW	1500	0.3
		W	1403	0.3		W	1574	0.3			W	1894	0.3		W	1800	0.3
		SW	115	0.3		SW	2185	0.3			SW	140	0.3		SW	* 6517	0.3

Table A1. *Cont.*

	Point	Measurement		Simulation	Point	Measurement		Simulation		Point	Measurement		Simulation	Point	Measurement		Simulation
		NW	165	0.3		NW	1182	0.3			NW	421	* 81.8		NW	1645	0.3
	P17	W	1330	0.3	P37	W	2046	0.3		P17	W	1917	* 100.0	P37	W	1939	0.3
		SW	63	0.3		SW	53	0.3			SW	234	* 100.0		SW	35	0.3
2:00 ~ 2:30 PM		NW	191	0.3		NW	74	0.3	4:00 ~ 4:30 PM		NW	1821	* 81.8		NW	78	0.3
	P18	W	1037	0.3	P38	W	1400	0.3		P18	W	1775	* 100.0	P38	W	1726	0.3
		SW	44	0.3		SW	293	0.3			SW	179	* 100.0		SW	3109	0.3
		NW	882	0.3		NW	47	0.3			NW	1235	* 81.8		NW	1295	0.3
	P19	W	1293	0.3	P39	W	1674	0.3		P19	W	3443	* 100.0	P39	W	1938	0.3
		SW	2069	0.3		SW	40	0.3			SW	* 5605	* 100.0		SW	324	0.3
		NW	1053	0.3		NW	1165	0.3			NW	1720	* 81.8		NW	1614	0.3
	P20	W	1109	0.3	P40	W	1804	0.3		P20	W	2501	* 100.0	P40	W	2302	0.3
		SW	1802	0.3		SW	138	0.3			SW	* 8235	* 100.0		SW	351	0.3

*: 4000 cd/m^2 or 45% DGP ≤ result.

Appendix B

Table A2. Comparison of the luminance measurements and DGP simulations in Space B. Unit: cd/m^2 (measurement) and DGP (%) (simulation).

	Point		Measurement	Simulation	Point		Measurement	Simulation		Point		Measurement	Simulation	Point		Measurement	Simulation
2:00 ~ 2:30 PM	P1	NW	63	0.3	P15	NW	856	0.3	4:00 ~ 4:30 PM	P1	NW	132	* 82.2	P15	NW	1383	* 82.2
		W	1114	0.3		W	1115	0.3			W	1945	* 100.0		W	2285	* 100.0
		SW	1517	0.3		SW	1333	0.3			SW	* 4677	* 100.0		SW	* 4821	* 100.0
	P2	NW	500	0.3	P16	NW	250	0.3		P2	NW	1176	* 82.2	P16	NW	959	* 82.2
		W	1136	0.3		W	1327	0.3			W	2105	* 100.0		W	2348	* 100.0
		SW	1918	0.3		SW	1981	0.3			SW	* 5899	* 100.0		SW	* 4426	* 100.0
	P3	NW	865	0.3	P17	NW	830	0.3		P3	NW	1408	0.3	P17	NW	1213	* 82.2
		W	1139	0.3		W	1182	0.3			W	2523	0.3		W	2425	* 100.0
		SW	1628	0.3		SW	2058	0.3			SW	3629	0.3		SW	* 5503	* 100.0
	P4	NW	40	0.3	P18	NW	1152	0.3		P4	NW	172	* 82.2	P18	NW	1544	* 79.9
		W	139	0.3		W	1576	* 100.0			W	135	* 100.0		W	2309	* 100.0
		SW	775	0.3		SW	474	* 100.0			SW	* 10,180	* 100.0		SW	340	* 100.0
	P5	NW	939	0.3	P19	NW	732	0.3		P5	NW	1186	* 82.2	P19	NW	1028	0.3
		W	1176	0.3		W	1137	0.3			W	1886	* 100.0		W	1988	0.3
		SW	1886	0.3		SW	1504	0.3			SW	* 6277	* 100.0		SW	* 4041	0.3
	P6	NW	777	0.3	P20	NW	1127	0.3		P6	NW	1345	0.3	P20	NW	1544	0.3
		W	1209	0.3		W	1201	0.3			W	2481	0.3		W	1974	0.3
		SW	2145	0.3		SW	1373	0.3			SW	* 7502	0.3		SW	2912	0.3
	P7	NW	157	0.3	P21	NW	938	0.3		P7	NW	127	* 82.2	P21	NW	1278	0.3
		W	1405	0.3		W	1097	0.3			W	2290	* 100.0		W	2387	0.3
		SW	2079	0.3		SW	1580	0.3			SW	* 4602	* 100.0		SW	* 4581	0.3
	P8	NW	648	0.3	P22	NW	727	0.3		P8	NW	768	* 82.2	P22	NW	1235	0.3
		W	1590	0.3		W	1298	0.3			W	2349	* 100.0		W	2245	0.3
		SW	2889	0.3		SW	1638	0.3			SW	3034	* 100.0		SW	* 4216	0.3

Table A2. *Cont.*

	Point		Measurement	Simulation	Point		Measurement	Simulation		Point		Measurement	Simulation	Point		Measurement	Simulation
		NW	976	0.3		NW	1023	0.3			NW	1474	0.3		NW	1271	0.3
	P9	W	1463	* 100.0	P23	W	1288	0.3		P9	W	2267	0.3	P23	W	1986	0.3
		SW	1983	* 100.0		SW	1620	0.3			SW	* 7274	0.3		SW	3350	0.3
		NW	200	0.3		NW	891	0.3			NW	267	* 82.2		NW	1328	0.3
	P10	W	1082	0.3	P24	W	1147	0.3		P10	W	2415	* 100.0	P24	W	2120	0.3
		SW	1582	0.3		SW	1884	0.3			SW	* 5429	* 100.0		SW	* 6176	0.3
2:00 ~ 2:30 PM		NW	800	0.3		NW	741	0.3	4:00 ~ 4:30 PM		NW	1251	* 82.2		NW	1280	0.3
	P11	W	1140	0.3	P25	W	1304	0.3		P11	W	2062	* 100.0	P25	W	2714	0.3
		SW	1458	0.3		SW	1994	0.3			SW	* 4441	* 100.0		SW	* 6492	0.3
		NW	870	0.3		NW	982	0.3			NW	1451	* 82.2		NW	1344	0.3
	P12	W	1106	0.3	P26	W	1377	0.3		P12	W	2079	* 100.0	P26	W	2237	0.3
		SW	124	0.3		SW	2735	0.3			SW	186	* 100.0		SW	* 5643	0.3
		NW	637	0.3		NW	944	0.3			NW	1126	* 82.2		NW	1570	* 79.9
	P13	W	1251	0.3	P27	W	1644	* 100.0		P13	W	3604	* 100.0	P27	W	1622	* 100.0
		SW	1747	0.3		SW	3140	* 100.0			SW	* 8360	* 100.0		SW	* 12,600	* 100.0
		NW	884	0.3							NW	1060	* 82.2				
	P14	W	1175	0.3						P14	W	2053	* 100.0				
		SW	1723	0.3							SW	* 5195	* 100.0				

*: 4000 cd/m^2 or 45% DGP $\leq$ result.

Appendix C

Table A3. Comparison of the luminance measurements and DGP simulations in Space C. Unit: cd/m^2 (measurement) and DGP (%) (simulation).

Time	Point	Measurement	Simulation	Point	Measurement	Simulation	Time	Point	Measurement	Simulation	Point	Measurement	Simulation
2:00 ~ 2:30 PM	P1	NW 632	0.3	P21	NW 1366	0.3	4:00 ~ 4:30 PM	P1	NW 412	0.3	P21	NW 2509	* 83.0
		W 1282	* 100.0		W * 5502	0.3			W 3130	0.3		W * 5564	* 100.0
		SW 2999	* 100.0		SW * 4182	0.3			SW * 6086	0.3		SW * 8490	* 100.0
	P2	NW 1439	0.3	P22	NW 3106	0.3		P2	NW 1449	* 83.0	P22	NW 3002	* 83.0
		W 2421	* 100.0		W * 4252	0.3			W 3034	* 100.0		W * 5220	* 100.0
		SW * 4292	* 100.0		SW * 4218	0.3			SW * 6018	* 100.0		SW * 5241	* 100.0
	P3	NW 1865	0.3	P23	NW 2750	0.3		P3	NW 1709	* 83.0	P23	NW 3575	0.3
		W 3495	* 100.0		W 2060	0.3			W * 5227	* 100.0		W 3741	0.3
		SW * 4624	* 100.0		SW 3910	0.3			SW * 6445	* 100.0		SW 1502	0.3
	P4	NW 1242	0.3	P24	NW 2058	0.3		P4	NW 3331	0.3	P24	NW 3141	0.3
		W 3137	* 100.0		W 3047	0.3			W * 4083	0.3		W * 5189	0.3
		SW 421	* 100.0		SW 25	0.3			SW 78	0.3		SW 23	0.3
	P5	NW 104	0.3	P25	NW 98	0.3		P5	NW 148	* 83.0	P25	NW 619	0.3
		W 3503	* 100.0		W 2579	0.3			W * 4130	* 100.0		W 3026	0.3
		SW 2372	* 100.0		SW 82	0.3			SW * 5163	* 100.0		SW * 7865	0.3
	P6	NW 2424	0.3	P26	NW 1048	0.3		P6	NW 2807	* 83.0	P26	NW 1958	0.3
		W 3517	* 100.0		W 2075	0.3			W 1880	* 100.0		W 3351	0.3
		SW 2759	* 100.0		SW 3876	0.3			SW * 7238	* 100.0		SW * 11,750	0.3
	P7	NW 14	0.3	P27	NW 2464	0.3		P7	NW 27	0.3	P27	NW 3504	0.3
		W 10	* 100.0		W 2790	0.3			W 69	0.3		W * 6245	0.3
		SW 13	* 100.0		SW 2041	0.3			SW 24	0.3		SW * 7674	0.3
	P8	NW 2686	0.3	P28	NW 1321	0.3		P8	NW 2413	0.3	P28	NW 2564	0.3
		W 2593	0.3		W * 4001	0.3			W * 5005	0.3		W 2939	0.3
		SW 3978	0.3		SW 2111	0.3			SW * 4470	0.3		SW * 6688	0.3

Table A3. *Cont.*

	Point	Measurement		Simulation	Point	Measurement		Simulation		Point	Measurement		Simulation	Point	Measurement		Simulation
		NW	257	0.3		NW	1500	0.3			NW	508	* 83.0		NW	1450	0.3
	P9	W	2343	0.3	P29	W	* 4606	0.3		P9	W	2577	* 100.0	P29	W	* 5959	0.3
		SW	2271	0.3		SW	2026	0.3			SW	* 8941	* 100.0		SW	* 5650	0.3
		NW	620	0.3		NW	3028	0.3			NW	620	* 83.0		NW	2797	0.3
	P10	W	2701	0.3	P30	W	3189	0.3		P10	W	3474	* 100.0	P30	W	* 4970	0.3
		SW	* 4293	0.3		SW	3540	0.3			SW	* 11,640	* 100.0		SW	* 6339	0.3
		NW	1990	0.3		NW	125.0	0.3			NW	3071	* 83.0		NW	124	0.3
	P11	W	3311	0.3	P31	W	89.0	0.3		P11	W	* 6338	* 100.0	P31	W	90	0.3
		SW	3268	0.3		SW	41.0	0.3			SW	* 6101	* 100.0		SW	79	0.3
2:00 ~ 2:30 PM		NW	2307	0.3		NW	2528.0	0.3	4:00 ~ 4:30 PM		NW	2093	* 83.0		NW	2041	0.3
	P12	W	3046	0.3	P32	W	3348.0	0.3		P12	W	* 5308	* 100.0	P32	W	* 5389	0.3
		SW	89	0.3		SW	143.0	0.3			SW	125	* 100.0		SW	217	0.3
		NW	2708	0.3		NW	191.0	0.3			NW	2250	* 83.0		NW	313	0.3
	P13	W	* 4914	0.3	P33	W	1820.0	0.3		P13	W	3082	* 100.0	P33	W	* 4086	0.3
		SW	3175	0.3		SW	* 4479.0	0.3			SW	* 8357	* 100.0		SW	* 7851	0.3
		NW	3120	0.3		NW	31.0	0.3			NW	3101	* 83.0		NW	43	0.3
	P14	W	2269	0.3	P34	W	1384.0	0.3		P14	W	* 4161	* 100.0	P34	W	1816	0.3
		SW	2271	0.3		SW	3898.0	0.3			SW	* 6421	* 100.0		SW	* 9640	0.3
		NW	2220	0.3		NW	550.0	0.3			NW	2983	* 83.0		NW	1068	0.3
	P15	W	2651	0.3	P35	W	2909.0	0.3		P15	W	* 4845	* 100.0	P35	W	* 5147	0.3
		SW	2851	0.3		SW	2289.0	0.3			SW	* 6041	* 100.0		SW	3457	0.3
		NW	2103	0.3		NW	1188.0	0.3			NW	1850	0.3		NW	1637	0.3
	P16	W	2826	0.3	P36	W	* 5030.0	0.3		P16	W	3559	0.3	P36	W	* 4860	0.3
		SW	281	0.3		SW	2199.0	0.3			SW	310	0.3		SW	* 4238	0.3

Table A3. *Cont.*

	Point	Measurement		Simulation	Point	Measurement		Simulation		Point	Measurement		Simulation	Point	Measurement		Simulation
		NW	348	0.3		NW	1491.0	0.3			NW	637	* 83.0		NW	1419	0.3
	P17	W	3754	0.3	P37	W	2809.0	0.3		P17	W	3300	* 100.0	P37	W	* 4050	0.3
		SW	* 5107	0.3		SW	2220.0	0.3			SW	* 10,860	* 100.0		SW	* 4815	0.3
2:00		NW	1274	0.3		NW	1249.0	0.3	4:00		NW	1823	* 83.0		NW	2283	0.3
~	P18	W	3393	0.3	P38	W	3470.0	0.3	~	P18	W	* 4144	* 100.0	P38	W	3889	0.3
2:30 PM		SW	* 4695	0.3		SW	* 4282.0	0.3	4:30 PM		SW	* 8703	* 100.0		SW	* 4824	0.3
		NW	2950	0.3		NW	3153	* 83.0			NW	2887	0.3				
	P19	W	3289	0.3	P19	W	85.0	0.3		P39	W	* 6217	* 100.0		W	131	0.3
		SW	1904	0.3		SW	93.0	0.3			SW	* 5681	* 100.0		SW	249	0.3
		NW	1399	0.3		NW	33.0	0.3			NW	2565	* 83.0		NW	54	0.3
	P20	W	3358	0.3	P40	W	2294.0	0.3		P20	W	* 4323	* 100.0	P40	W	* 4645	0.3
		SW	* 4803	0.3		SW	38.0	0.3			SW	* 8658	* 100.0		SW	61	0.3

*: 4000 cd/m^2 or 45% DGP $\leq$ result.

References

1. Brainard, G.C.; Hanifin, J.P.; Rollag, M.D.; Greeson, J.; Byrne, B.; Glickman, G.; Sanford, B. Human melatonin regulation is not mediated by the three cone photopic visual system. *J. Clin. Endocrinol. Metab.* **2001**, *86*, 433–436.
2. Cajochen, C.; Zeitzer, J.M.; Czeisler, C.A.; Dijk, D.J. Dose-response relationship for light intensity and ocular and electroencephalographic correlates of human alertness. *Behav. Brain Res.* **2000**, *115*, 75–83. [CrossRef]
3. Lockley, S.W.; Brainard, G.C.; Czeisler, C.A. High sensitivity of the human circadian melatonin rhythm to resetting by short wavelength light. *J. Clin. Endocrinol. Metab.* **2003**, *88*, 4502–4505. [CrossRef]
4. Rea, M.S.; Figueiro, M.G.; Bullough, J.D.; Bierman, A. A model of phototransduction by the human circadian system. *Brain Res. Rev.* **2005**, *50*, 213–228. [CrossRef]
5. Viola, A.U.; James, L.M.; Schlangen, L.J.; Dijk, D.J. Blue-enriched white light in the workplace improves self-reported alertness, performance and sleep quality. *Scand. J. Work Environ. Health* **2008**, *34*, 297–306. [CrossRef]
6. Vetter, C.; Pattison, P.M.; Houser, K.; Herf, M.; Phillips, A.J.; Wright, K.P.; Glickman, G. A review of human physiological responses to light: Implications for the development of integrative lighting solutions. *Leukos* **2022**, *18*, 387–414. [CrossRef]
7. Lu, M.; Hu, S.; Mao, Z.; Liang, P.; Xin, S.; Guan, H. Research on work efficiency and light comfort based on EEG evaluation method. *Build. Environ.* **2020**, *183*, 107122. [CrossRef]
8. Goodman, T.M. Measurement and specification of lighting: A look at the future. *Light. Res. Technol.* **2009**, *41*, 229–243. [CrossRef]
9. Hassan, M.U.; Angelaki, S.; Alfaro, C.V.L.; Major, P.; Styve, A.; Alaliyat, S.A.A.; da Silva Torres, R. Digital Twins for Lighting Analysis: Literature Review, Challenges, and Research Opportunities. In Proceedings of the 36th International ECMS Conference on Modelling and Simulation, Alesund, Norway, 30 May–3 June 2022; ECMS: Caserta, Italy, 2022; Volume 36, pp. 226–235.
10. Ricciardi, P.; Buratti, C. Environmental quality of university classrooms: Subjective and objective evaluation of the thermal, acoustic, and lighting comfort conditions. *Build. Environ.* **2018**, *127*, 23–36. [CrossRef]
11. United Nation General Assembly. Transforming Our World: The 2030 Agenda for Sustainable Development. Available online: https://www.un.org/en/development/desa/population/migration/generalassembly/docs/globalcompact/A_RES_70_1_E.pdf (accessed on 11 October 2023).
12. Solemma. What is ClimateStudio? Available online: https://www.solemma.com/climatestudio (accessed on 5 April 2023).
13. Nielsen, M.V.; Svendsen, S.; Jensen, L.B. Quantifying the potential of automated dynamic solar shading in office buildings through integrated simulations of energy and daylight. *Sol. Energy* **2011**, *85*, 757–768. [CrossRef]
14. Boubekri, M.; Lee, J.; MacNaughton, P.; Woo, M.; Schuyler, L.; Tinianov, B.; Satish, U. The impact of optimized daylight and views on the sleep duration and cognitive performance of office workers. *Int. J. Environ. Res. Public Health* **2020**, *17*, 3219. [CrossRef]
15. Konis, K. A novel circadian daylight metric for building design and evaluation. *Build. Environ.* **2017**, *113*, 22–38. [CrossRef]
16. Bellia, L.; Pedace, A.; Barbato, G. Daylighting offices: A first step toward an analysis of photobiological effects for design practice purposes. *Build. Environ.* **2014**, *74*, 54–64. [CrossRef]
17. Lee, J.; Boubekri, M. Impact of daylight exposure on health, well-being and sleep of office workers based on actigraphy, surveys, and computer simulation. *J. Green Build.* **2020**, *15*, 19–42. [CrossRef]
18. Heerwagen, J.H.; Orians, G.H. Adaptations to windowlessness: A study of the use of visual decor in windowed and windowless offices. *Environ. Behav.* **1986**, *18*, 623–639. [CrossRef]
19. Boubekri, M.; Hull, R.B.; Boyer, L.L. Impact of window size and sunlight penetration on office workers' mood and satisfaction: A novel way of assessing sunlight. *Environ. Behav.* **1991**, *23*, 474–493. [CrossRef]
20. Heschong, L. Daylighting and human performance. *ASHRAE J.* **2002**, *44*, 65–67.
21. Van Den Wymelenberg, K. Patterns of occupant interaction with window blinds: A literature review. *Energy Build.* **2012**, *51*, 165–176. [CrossRef]
22. Wang, N.; Boubekri, M. Design recommendations based on cognitive, mood and preference assessments in a sunlit workspace. *Light. Res. Technol.* **2011**, *43*, 55–72. [CrossRef]
23. Gou, Z.; Lau, S.S.Y.; Qian, F. Comparison of mood and task performance in naturally-lit and artificially-lit environments. *Indoor Built Environ.* **2015**, *24*, 27–36. [CrossRef]
24. Wienold, J.; Christoffersen, J. *Towards a New Daylight Glare Rating*; Lux Europa: Berlin, Germany, 2005; pp. 157–161.
25. Suk, J.Y.; Schiler, M.; Kensek, K. Investigation of existing discomfort glare indices using human subject study data. *Build. Environ.* **2017**, *113*, 121–130. [CrossRef]
26. Veitch, J.A.; Newsham, G.R. Preferred luminous conditions in open-plan offices: Research and practice recommendations. *Int. J. Light. Res. Technol.* **2000**, *32*, 199–212. [CrossRef]
27. Schiler, M. Toward a definition of glare: Can qualitative issues be quantified? In Proceedings of the 2nd EAAE–ARCC Conference on Architectural Research, Paris, France, 4 July 2000.
28. Egan, M.D. *Concepts in Architectural Lighting*; McGraw-Hill: New York, NY, USA, 1983.
29. Wienold, J.; Christoffersen, J. Evaluation methods and development of a new glare prediction model for daylight environments with the use of CCD cameras. *Energy Build.* **2006**, *38*, 743–757. [CrossRef]
30. Solemma. Annual Glare. In ClimateStudio User Guide. Available online: https://climatestudiodocs.com/docs/annualGlare.html (accessed on 5 April 2023).
31. Bechthold, M.; King, N.; Kane, A.O.; Niemasz, J.; Reinhart, C. Integrated environmental design and robotic fabrication workflow for ceramic shading systems. *Autom. Robot. Build. Constr.* **2011**, *9*, 70–75.

32. Motevalian, E. Double Skin Facades Performance: Effects on Daylight and Visual Comfort in Office Spaces. Ph.D. Thesis, University of Southern California, Los Angeles, CA, USA, 2014.

33. Yun, G.; Yoon, K.C.; Kim, K.S. The influence of shading control strategies on the visual comfort and energy demand of office buildings. *Energy Build.* **2014**, *84*, 70–85. [CrossRef]

34. Wagdy, A.; Fathy, F. A parametric approach for achieving optimum daylighting performance through solar screens in desert climates. *J. Build. Eng.* **2015**, *3*, 155–170. [CrossRef]

35. Kong, Z.; Utzinger, M.; Liu, L. Solving glare problems in architecture through integration of HDR image technique and modeling with DIVA. In Proceedings of the 14th Conference of International Building Performance Simulation Association, Hyderabad, India, 7–9 December 2015; pp. 1221–1228.

36. Arango-Díaz, L. Deslumbramiento en ambientes educativos con muro calado en fachada. *Rev. AUS* **2016**, *20*, 62–69. [CrossRef]

37. Shin, C.; Collins, G. Daylight Glare Analysis for an All Glass Cathedral: Integrating Simulation with Common Sense to Improve Visual Comfort. *Proc. SimBuild.* **2016**, *6*, 267–274.

38. Gao, Y.; Dong, J.; Isabella, O.; Zeman, M.; Zhang, G.Q. Daylighting simulation and analysis of buildings with dynamic photovoltaic window shading elements. In Proceedings of the 2017 14th China International Forum on Solid State Lighting: International Forum on Wide Bandgap Semiconductors China (SSLChina: IFWS), Beijing, China, 1–3 November 2017; IEEE: New York, NY, USA, 2017; pp. 52–55.

39. Sherif, A.; Mahmoud, A.; ElSharkawy, M.; Eissa, A. Parametric Configuration of Window Light Shelves for Daylighting of Hospital Patient Rooms under a Desert Clear Sky. *Proceeding PLEA* **2017**, *2*, 3380–3387.

40. Wagdy, A.; Sherif, A.; Sabry, H.; Arafa, R.; Mashaly, I. Daylighting simulation for the configuration of external sun-breakers on south oriented windows of hospital patient rooms under a clear desert sky. *Sol. Energy* **2017**, *149*, 164–175. [CrossRef]

41. Sharma, L.; Kishan Lal, K.; Rakshit, D. Evaluation of impact of passive design measures with energy saving potential through estimation of shading control for visual comfort. *J. Build. Phys.* **2018**, *42*, 220–238. [CrossRef]

42. Bian, Y.; Leng, T.; Ma, Y. A proposed discomfort glare evaluation method based on the concept of 'adaptive zone'. *Build Environ.* **2018**, *143*, 306–317. [CrossRef]

43. Tabadkani, A.; Banihashemi, S.; Hosseini, M.R. Daylighting and visual comfort of oriental sun responsive skins: A parametric analysis. *Build. Simul.* **2018**, *11*, 663–676. [CrossRef]

44. Sharma, L.; Rakshit, D. Visual comfort based algorithmic control for roller shade and assessment of potential energy savings. In *Applications of Solar Energy*, 1st ed.; Tyagi, H., Agarwal, A., Chakraborty, P., Powar, S., Eds.; Springer: Singapore, 2018; pp. 295–316.

45. Ayçam, İ.; Ceylan, Ö. Analysis of Daylight Control in Advanced Façade Systems for Office Module in Ankara. In *Proceedings of the 3rd International Sustainable Buildings Symposium (ISBS 2017)*; Fırat, S., Kinuthia, J., Abu-Tair, A., Eds.; Springer: Cham, Germany, 2018; Volume 13, pp. 359–377.

46. Lee, S.; Lee, K.S. A Study on the improvement of the evaluation scale of discomfort glare in educational facilities. *Energies* **2019**, *12*, 3265. [CrossRef]

47. Pagliolico, S.L.; Verso, V.R.L.; Zublena, M.; Giovannini, L. Preliminary results on a novel photo-bio-screen as a shading system in a kindergarten: Visible transmittance, visual comfort and energy demand for lighting. *Sol. Energy* **2019**, *185*, 41–58. [CrossRef]

48. Mesloub, A.; Ghosh, A.; Touahmia, M.; Albaqawy, G.A.; Noaime, E.; Alsolami, B.M. Performance analysis of photovoltaic integrated shading devices (PVSDs) and semi-transparent photovoltaic (STPV) devices retrofitted to a prototype office building in a hot desert climate. *Sustainability* **2020**, *12*, 10145. [CrossRef]

49. Sun, Y.; Liu, X.; Qu, W.; Cao, G.; Zou, N. Analysis of daylight glare and optimal lighting design for comfortable office lighting. *Optik* **2020**, *206*, 164291. [CrossRef]

50. Srisamranrungruang, T.; Hiyama, K. Balancing of natural ventilation, daylight, thermal effect for a building with double-skin perforated facade (DSPF). *Energy Build.* **2020**, *210*, 109765. [CrossRef]

51. Triantafyllidou, E.F.; Michael, A.G. The impact of installing a concave curved profile blind to a glass window for visual comfort in office buildings. *Procedia. Manuf.* **2020**, *44*, 269–276. [CrossRef]

52. Kiliç, Z.A.; Yener, A.K. Determining Proper Daylighting Design Solution for Visual Comfort and Lighting Energy Efficiency: A Case Study for High-Rise Residential Building. *J. Phys. Conf. Ser.* **2021**, *2069*, 012156. [CrossRef]

53. Özdemir, H.; Çakmak, B.Y. Evaluation of Daylight and Glare Quality of Office Spaces with Flat and Dynamic Shading System Facades in Hot Arid Climate. *J. Daylighting* **2022**, *9*, 197–208. [CrossRef]

54. Mesloub, A.; Ghosh, A.; Touahmia, M.; Albaqawy, G.A.; Alsolami, B.M.; Ahriz, A. Assessment of the overall energy performance of an SPD smart window in a hot desert climate. *Energy* **2022**, *252*, 124073. [CrossRef]

55. Navabi, D.; Amini, Z.; Rahmati, A.; Tahbaz, M.; Butt, T.E.; Sharifi, S.; Mosavi, A. Developing light transmitting concrete for energy saving in buildings. *Case Stud. Constr. Mater.* **2023**, *18*, e01969. [CrossRef]

56. Sui, G.; Liu, J.; Leng, J.; Yu, F. Daylighting performance assessment of traditional skywell dwellings: A case study in Fujian, China. *J. Build. Eng.* **2023**, *68*, 106028. [CrossRef]

57. Sorooshnia, E.; Rashidi, M.; Rahnamayiezekavat, P.; Rezaei, F.; Samali, B. Optimum external shading system for counterbalancing glare probability and daylight illuminance in Sydney's residential buildings. *Eng. Constr. Archit. Manag.* **2023**, *30*, 296–320. [CrossRef]

58. Hassan, F.H.; Ali, K.A.; Ahmed, S.A. Biomimicry as an Approach to Improve Daylighting Performance in Office Buildings in Assiut City, Egypt. *J. Daylighting.* **2023**, *10*, 1–16. [CrossRef]

59.　Taleb, H.M.; Moarbes, R. Improving illuminance performance by implementing a kinetic façade system: Case study of office building in Dubai. *J. Asian Archit. Build. Eng.* **2023**, *22*, 2809–2826. [CrossRef]

60.　Suk, J.Y.; Schiler, M.; Kensek, K. Development of new daylight glare analysis methodology using absolute glare factor and relative glare factor. *Energy Build.* **2013**, *64*, 113–122. [CrossRef]

61.　He, S.; Li, H.; Yan, Y.; Cai, H. Calibrating lighting simulation with panoramic high dynamic range imaging. *J. Build. Perform. Simul.* **2023**, 1–20. [CrossRef]

62.　Safranek, S.; Davis, R.G. Sources of error in HDRI for luminance measurement: A review of the literature. *Leukos* **2021**, *17*, 187–208. [CrossRef]

63.　Konika Minolta Sensing Americas Inc. CS-150 Luminance and Color Meter. Available online: https://sensing.konicaminolta.us/us/products/cs-150-luminance-and-color-meter/ (accessed on 2 February 2023).

64.　Korea Meteorological Administration. Observation and Climate. Available online: https://web.kma.go.kr/w/obs-climate/land/past-obs/obs-by-element.do?stn=108&yy=2023&obs=59 (accessed on 1 March 2023).

65.　Konika Minolta Sensing Americas Inc. CL-500A Illuminance Spectrophotometer. Available online: https://sensing.konicaminolta.us/us/products/cl-500a-illuminance-spectrophotometer/ (accessed on 2 February 2023).

66.　Suk, J.Y.; Schiler, M.; Kensek, K. Absolute glare factor and relative glare factor based metric: Predicting and quantifying levels of daylight glare in office space. *Energy Build.* **2016**, *130*, 8–19. [CrossRef]

67.　Purves, D.; Augustine, G.J.; Fitzpatrick, D. Anatomical distribution of rods and cones. In *Neuroscience*, 2nd ed.; Sinauer Associates: Sunderland, MA, USA, 2001. Available online: https://www.ncbi.nlm.nih.gov/books/NBK10848/ (accessed on 15 January 2023).